CFD Letters

Journal homepage:
https://semarakilmu.com.my/journals/index.php/CFD_Letters/index
ISSN: 2180-1363

Effects of Homogeneous and Inhomogeneous Roughness on the Ship Resistance

Rajabal Akbar[1], I Ketut Suastika[2,*], I Ketut Aria Pria Utama[2]

[1] Department of Ocean Engineering, Faculty of Marine Technology, Institut Teknologi Sepuluh Nopember (ITS), Surabaya 60111, Indonesia
[2] Department of Naval Architecture, Faculty of Marine Technology, Institut Teknologi Sepuluh Nopember (ITS), Surabaya 60111, Indonesia

ARTICLE INFO

Article history:
Received 6 June 2024
Received in revised form 8 July 2024
Accepted 9 August 2024
Available online 31 October 2024

Keywords:
CFD; homogeneous roughness; inhomogeneous roughness; KCS; RANS; ship resistance

ABSTRACT

Ship hull roughness can significantly increase the ship resistance. The roughness caused by biofouling attached to the ship hull is not uniform but has a random distribution. The purpose of this study is to investigate how the inhomogeneous surface roughness distribution affects the ship resistance and the various resistance components. The KRISO container ship (KCS) is considered as a case study. To model the inhomogeneous surface roughness, the ship hull is divided into three segments with equal wetted surface area. Combinations of three roughness heights, denoted as P, Q, and R with k_s values of 125 µm, 269 µm, and 425 µm, respectively, are considered to obtain homogeneous and inhomogeneous roughness arrangements (PPP, QQQ, RRR, PQR, PRQ, QPR, QRP, RPQ, and RQP). CFD method is utilized in this study, utilizing RANS equations and k-ω SST turbulence model. A VoF method is used to model the free surface. CFD simulation results show that for the homogeneous roughness, the total resistance coefficient C_T increases with increasing k_s (PPP < QQQ < RRR), as expected. For the inhomogeneous roughness, the friction resistance coefficient C_F increases in the order PQR < PRQ < QPR < QRP < RPQ < RQP, consistent with results from earlier studies. In all the cases, the friction resistance (C_F) is the dominant component of the total resistance. As Re increases from 2.2 x 10^9 to 2.7 x 10^9, the percentage of the friction resistance decreases, while the percentage of the wave resistance increases. The viscous-pressure resistance decreases slightly as Re increases from 2.2 x 10^9 to 2.7 x 10^9.

1. Introduction

The shipping sector is currently facing a significant environmental issue as it transitions to a low-carbon, zero-pollution future. The International Maritime Organization (IMO) established a decarbonization initiative for international shipping in April 2018 to reduce carbon emissions by at least 50% by 2050 compared to 2008 [1]. The solution to this issue is that the shipping industry is required to design ships with the ability to reduce energy requirements, such as by increasing engine efficiency. In ship design, the issue of resistance is a crucial aspect [2]. Ship resistance is correlated with the ship propulsion (powering) used to reach a certain speed to increase engine efficiency [3].

* *Corresponding author.*
E-mail address: suastika@its.ac.id (I Ketut Suastika)

https://doi.org/10.37934/cfdl.17.3.7794

It is common knowledge that any object in motion experiences a resisting force, commonly called resistance. A low-resistance ship is a design goal because it causes less energy consumption, thus saving fuel by reducing the load on the propulsion engine. The friction resistance is a significant component of a bulk carrier's energy consumption. For example, in the study by Kodama *et al.,* [4] the friction resistance of a Very Large Crude Carrier (VLCC) is expected to be 80% to 90% of the ship's total resistance. Molland *et al.,* [5] discovered the potential for reducing resistance by optimizing hull-propeller-rudder interactions which has the potential to save power with optimized operational strategies, for example, those related to speed.

ITTC [6] encourages the development of methods to calculate the increase in frictional resistance of vessels due to surface roughness. The initial analysis is typically conducted to ascertain the roughness of sand grains that are analogous to high k relative to surface roughness, given that the surface roughness associated with biofouling attached to the ship's hull is inherently heterogeneous. The ITTC recommends the method developed by Bowden and Davidson [7], which was later refined by Townsin [8], for calculating the increase in frictional resistance of vessels due to biofouling. The roughness effect on ship resistance can be accurately predicted if the surface roughness function ΔU^+ is known [9]. Many researchers have adopted the procedure for Granville's law [10], and [11] because of its reliability and low cost [12]. For example, Ravenna *et al.,* [13] investigated the effect of heterogeneous roughness on ship resistance using the Granville similarity, and Suastika *et al.,* [14] determined the effect of inhomogeneous roughness on drag penalty using the Granville method. Shapiro [15], and Candries [16] utilized the Granville equation to predict added resistance in large Reynolds numbers for rough flat plates. In Flack and Schultz's [17] study, the analysis from Granville was adopted and relied on the outer layer similarity in the mean flow for smooth and rough walls.

CFD is a powerful tool to investigate roughness effects on the ship resistance. Ship resistance predictions are more accurate when using CFD due to the 3D effect of the hull being modelled and the ability to model the ship at full scale so that it is close to actual conditions. Further, CFD can display visualizations in contours and vectors of desired hydrodynamic parameters. Due to the advantages of the CFD method, several recent studies have used the CFD approach to study the effect of roughness on ship resistance, as discussed by Demirel *et al.,* [18], and Song *et al.,* [19]. Hakim *et al.,* [20] conducted simulations using RANS equations to determine the resistance of a newly cleaned and painted hull (orange peel roughness).

Ravenna *et al.,* [13] and Song *et al.,* [21, 22] explored the impact of roughness distribution on the ship resistance and presented results of C_F, C_P, and C_T. In their study, the ship hull is divided into three segments, but the area of the segments is not the same. This study investigates the various components contributing to the total resistance (C_T), including friction resistance (C_F), wave resistance (C_W), and viscous pressure resistance (C_{VP}) resulting from smooth, homogeneous and inhomogeneous roughness. This allows for a more detailed assessment of the factors contributing to total resistance.

The objective of this study is to investigate the effects of homogeneous and inhomogeneous roughness on the ship resistance. The KCS hull is considered as a case study. To model the inhomogeneous surface roughness, the ship hull is divided into three segments with equal wetted surface area. Combinations of three roughness heights, denoted as P, Q, and R with k_s values of 125 µm, 269 µm, and 425 µm, respectively, are considered to obtain homogeneous and inhomogeneous roughness arrangements (PPP, QQQ, RRR, PQR, PRQ, QPR, QRP, RPQ, and RQP). CFD method is utilized in this study, utilizing RANS equations and k-ω SST turbulence model. A VoF method is used to model the free surface. Two Reynolds numbers are considered, namely, Re = 2.2 x 10^9 and 2.7 x 10^9.

2. Methodology

This study utilizes a CFD method to investigate the effects of homogeneous and inhomogeneous roughness on the ship resistance. The CFD method discretizes the RANS equations on a grid, resulting in a system of algebraic equations that are solved using numerical methods utilizing an iterative solution method [23]. The finite volume method is employed for the discretization. The RANS equations consist of nonlinear Reynolds stresses, requiring further modeling, namely a turbulence model. The k-ω SST (Shear Stress Transport) turbulence model [24] is used in this study.

2.1 RANS Equations

The equations governing turbulent flows are the conservation equations of mass, momentum, and energy. This study uses the RANS model to simulate the turbulent flow over the ship hull. For incompressible flows without heat transfer, only the mass and momentum equations are applied. These are given, respectively, in Eq. (1) and Eq. (2):

$$\nabla.[\rho U] = 0 \tag{1}$$

$$\frac{\partial[\rho U]}{\partial t} + \nabla.\{\rho UU\} = -\nabla P + \left[\nabla.\left\{\bar{\tau}_{ij} - \rho\overline{u'u'}\right\}\right] + \rho g \tag{2}$$

The Reynolds stress $-\rho\overline{u'u'}$ in Eq. (2) is calculated by using the *k-ω* SST turbulence model [24], thereby closing the system of Eq. (1) and Eq. (2). This turbulence model, a combination of the *k-Ɛ* model, applied outside and in the outer region of the boundary layer, and the *k-ω* model applied in the inner region of the boundary layer, can predict flow separations accurately. Flow simulations over rough surfaces are carried out by applying a roughness function [14].

Two-phase flow simulations with a free surface are carried out, with water below and air above the free surface, utilizing the volume of fluid (VoF) method [25]. Sea water and air at a temperature of 20°C are considered with density ρ = 1025 kg/m^3 and viscosity μ 1.0 × 10^{-3} Pa.s for the seawater, and ρ = 1.2 kg/m^3 and viscosity μ = 1.825 × 10^{-5} Pa.s for the air.

2.2 Geometrical Modelling and Roughness Arrangements

The principal particular of the KCS hull is summarized in Table 1. The hull geometry of the KCS is shown in Figure 1 and Figure 2. The surface roughnesses used in this study is similar to those reported by Suastika *et al.,* [14] namely with k_s 125 μm, 269 μm, and 425 μm. For the inhomogeneous roughness modelling, the KCS hull is divided into three segments: the fore-hull, midship, and aft-hull, with the same wetted surface area. The roughness arrangements on the KCS hull are shown in Figure 1 and Figure 2. Figure 1 illustrates the KCS hull with homogeneous roughness, including the KCS hull with smooth surface, while Figure 2 illustrates the inhomogeneous roughness arrangement.

Table 1
Principal particulars of the KCS in full-scale

Main feature	Symbol	Unit	Value
Length of water line	L_{WL}	m	232.5
Length between perpendiculars	Lpp	m	230
Breadth	B	m	32.2
Draught	T	m	10.8
Depth	H	m	19
Wetted Surface Area/ segment	WSA	m^2	3179
Displacement volume	∇	m^3	52030
Block coefficient	C_B	-	0.6505

Roughness modeling for KCS ships is performed by creating a design of roughness arrangements (PQR, PRQ, QPR, QRP, RPQ, RQP) with three roughness variations, namely low roughness P with k_s 125 µm, medium roughness Q with k_s 269 µm, and high roughness R with k_s 425 µm. The k_s values correspond to the ISO grade standard given in ISO 1302 [26]. Table 2 details the six inhomogeneous roughness arrangements, showing the distribution of roughness levels in the three segments. In addition to inhomogeneous roughness arrangements, simulations were also conducted with smooth surfaces (SSS) and homogeneous roughness arrangements (PPP, QQQ, RRR).

Table 2
Configuration of the roughness of the KCS Hull model

Model	Ship Segments		
	Aft-Hull	Midship	Fore-Hull
PQR	R	Q	P
PRQ	Q	R	P
QPR	R	P	Q
QRP	P	R	Q
RPQ	Q	P	R
RQP	P	Q	R

P (k_s = 125 µm), Q (k_s = 269 µm), R (k_s = 425 µm)

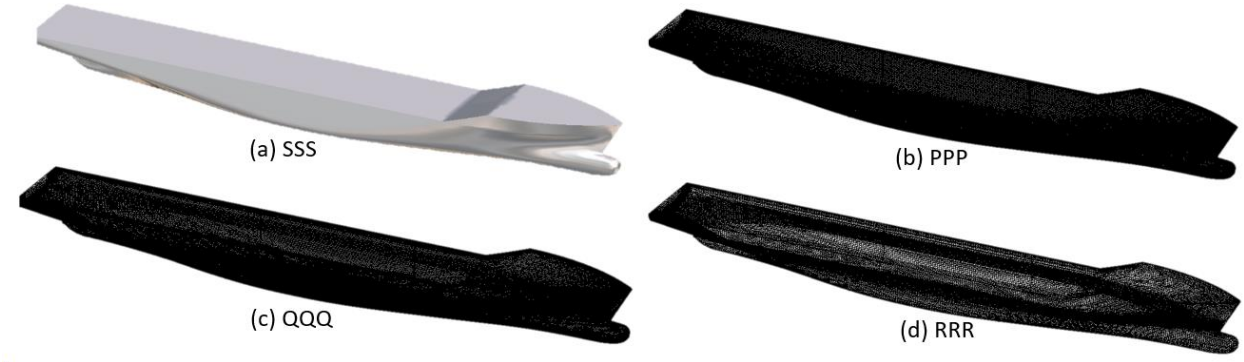

Fig. 1. Homogeneous roughness arrangements

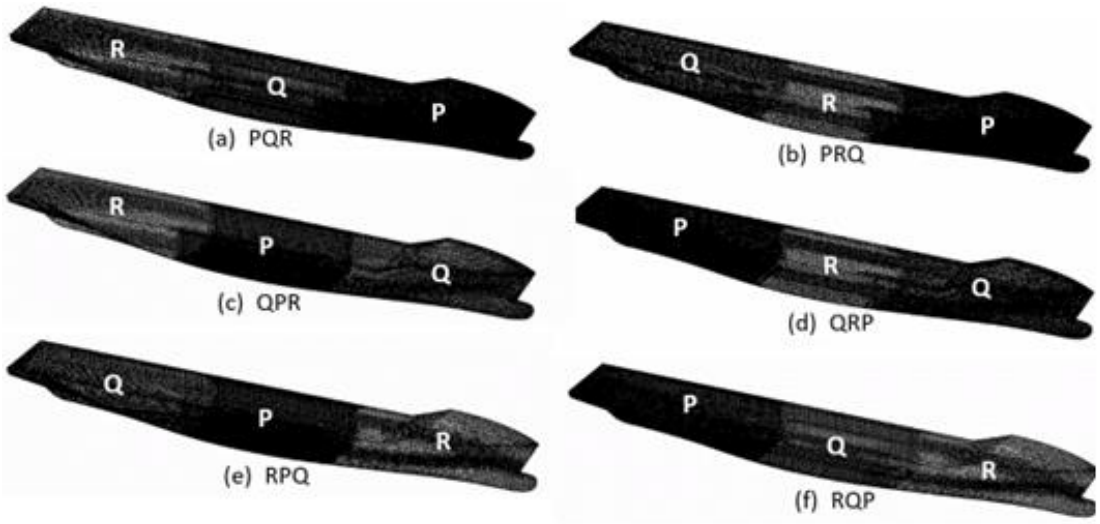

Fig. 2. Inhomogeneous roughness arrangements

2.3 Meshing and Grid Independence Tests

The computational domain with boundaries is shown in Figure 3. Figure 3 also shows the mesh structure used in the CFD simulations. The domain size and boundary conditions were selected following the ITTC recommendations. The boundary conditions are as follows. The no-slip condition is applied to the hull surface. The top, bottom, and side walls have been subjected to a slip-free ship condition. The middle plane of the hull or mirror is a condition of symmetry. At the inlet, it is set as the flow velocity being tested, while at the outlet, it is defined as hydrostatic pressure. These boundary condition settings follow the ITTC recommendations [27].

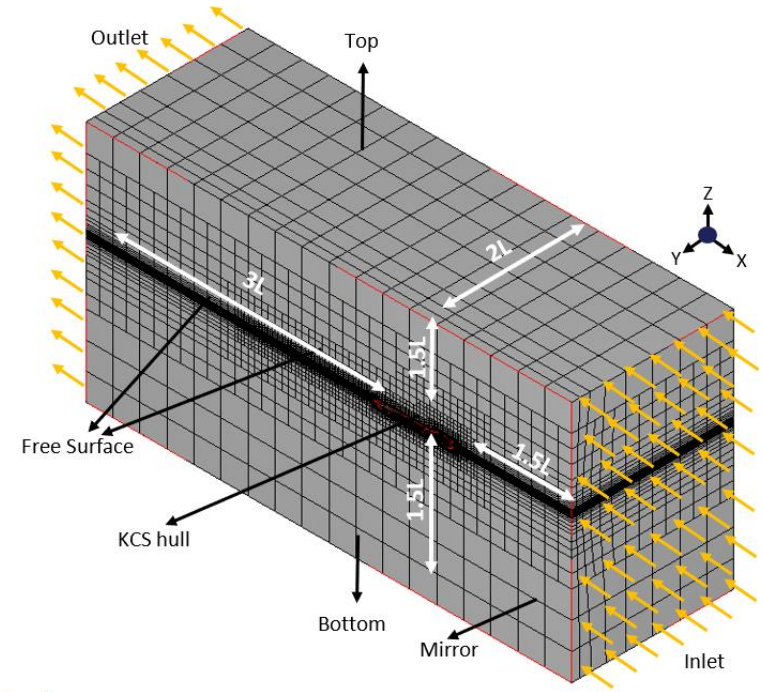

Fig. 3. Computational domain with boundaries

The mesh quality is crucial for achieving convergence and prescribed accuracy in CFD simulations. Thompson *et al.,* [28] and Wackers *et al.,* [29] provide detailed explanations of grid quality and quantity. A grid independence study was conducted on the KCS PPP roughness (k_s = 125 μm). The results of the grid independence tests are presented in Table 3 and Figure 4.

Table 3
Grid independence tests of KCS hull with homogenous roughness (PPP)

Run	Number of cells	C_T x 10^3	Percentage difference
1	246350	2.244	-
2	438090	2.053	9.30 %
3	947196	1.909	7.54 %
4	1798419	1.875	1.81 %
5	3189127	1.865	0.53 %
6	3745823	1.861	0.21 %

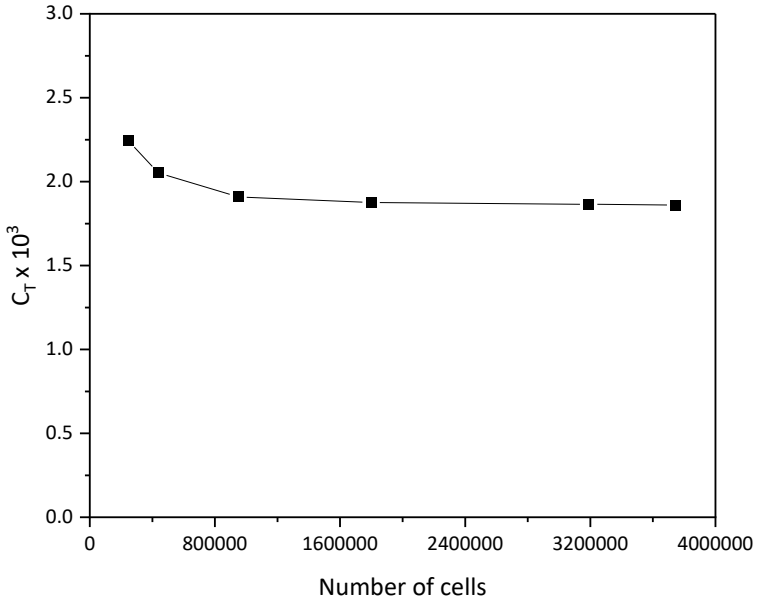

Fig. 4. Grid independence study

Table 3 and Figure 4 demonstrate that C_T decreases monotonically with increasing number of cells. Further, the percentage difference between run n+1 and run n also decreases monotonically with increasing number of cells. The percentage difference between run numbers 4 and 3 is less than 2%. Based on this result the number of cells of 1,798,419 is considered as the optimal number of cells. This indicates that the number of grids is sufficient to reduce computing costs and time [30], [31]. This finding follows the conclusions reached by Molland and Utama [31], which states that grid independence is optimal when the resistance difference between run n+1 and run n is less than 2%.

2.4 Verification and Validation

Verification of CFD results can be accomplished by determining the grid convergence index (GCI), employed to estimate grid error in this study. This method is based on the 2021 ITTC recommendations (7.5-03-01-01) [32], as demonstrated by Zingg [33]. Convergence studies were conducted using three different mesh resolutions: coarse, medium, and fine [34, 35]. The inflation

layer was maintained throughout the analysis, as the mesh resolution is based on standard wall calculations, as detailed in Table 4.

Table 4
The mesh resolution details

Parameter	Fine (1)	Medium (2)	Coarse (3)
Face sizing (m)	0.03	0.04	0.05
Number of Grids (NG)	3,189,127	1798419	947,196
Total resistance coefficient ($x10^{-3}$) (C_T)	1.865	1.875	1.909

To report the quality of grid convergence, the grid convergence index (GCI) is a standard method. A summary of the GCI study is presented in Table 5.

Table 5
Summary of the results of the GCI study

Outcome	Equation	Value
Difference of estimation	$\varepsilon_{21}=C_{T2}-C_{T1}$	0.01×10^{-3}
	$\varepsilon_{32}=C_{T3}-C_{T2}$	0.03×10^{-3}
Convergence ratio	$R_i= \varepsilon_{21}/ \varepsilon_{32}$	0.3
Refinement ratio	$r_i=r_{21}= r_{32}= (NG_2/NG_1)^{1/3}=(NG_3/NG_2)^{1/3}$	1.3
Order of accuracy	$p=\ln(\varepsilon_{32}/ \varepsilon_{21})/(\ln(ri))$	4.25
Extrapolated value	$C_{T,ext-21}=(((r_{21}^p)C_{T1})-C_{T2})/(r_{21}^p-1)$	1.860×10^{-3}
	$C_{T,ext-32}=(((r_{32}^p)C_{T2})-C_{T3})/(r_{32}^p-1)$	1.853×10^{-3}
Approximate relative error	$e_{a-21}=\lvert(C_{T1}-C_{T2})/C_{T1}\rvert$	0.5 %
	$e_{a-32}=\lvert(C_{T2}-C_{T3})/C_{T2}\rvert$	1.8 %
Extrapolated relative error	$e_{ext-21}=\lvert(C_{T,ext-21}-C_{T1})/C_{T,ext-21}\rvert$	0.2 %
	$e_{ext-32}=\lvert(C_{T,ext-32}-C_{T2})/C_{T,ext-32}\rvert$	1.1 %
Grid convergence index (GCI)	$GCI_{21}=(1,25.e_{a21})/ ((r_{21}^p)-1)$	0.2 %
	$GCI_{32}=(1,25.e_{a32})/ ((r_{32}^p)-1)$	1.4 %

Table 5 shows that the convergence study for structured grids shows monotonic convergence conditions, namely with a convergence ratio (R_i) of $0 < R_i < 1$. In this study, the R_i is 0.3. The difference of estimation (Ɛ) in this study is minimal, with a difference of ε_{21} for the fine grid and ε_{32} for the coarse grid, respectively 0.01×10^{-3} and 0.03×10^{-3}. The refinement ratio (r_i) with a recommended value close to $\sqrt{2}$ obtained in this study, with a value of 1.3. The order of accuracy (p) is 4.25. The extrapolated value ($C_{T,ext}$) exhibits a negligible discrepancy with the simulated C_T value, with a difference of 0.5 % for fine conditions ($C_{T,ext-21}$) and 2.1 % for coarse conditions ($C_{T,ext-32}$). In fine conditions, the approximate relative error (e_a) and extrapolated relative error (e_{ext}) are smaller than in coarse conditions, where e_{a-21} and e_{ext-21} are 0.5 % and 0.2 %, and e_{a-32} and e_{ext-32} are 1.8 % and 1.1 %. These error values are in accordance with ITTC recommendation (7.5-03-01-01) [32], which specifies a maximum of ±2.6%. In the GCI calculation, a safety factor (Fs = 1.25) is employed, which is obtained at 0.2 % for fine grids (GCI_{21}) and 1.4 % for coarse grids (GCI_{32}). The error and GCI on the fine grid result is smaller than the coarse grid, which indicates that the fine grid is more accurate with GCI below 1%, according to research by Adanta *et al.,* [35]*,* To achieve the most accurate predictions, the smallest grid size is utilized in subsequent simulations. The overall results were calculated based on the recommendations of the ITTC [32] which is in line with the research of Celik *et al.,* [34].

The CFD simulation results were validated by comparing them with the empirical equation recommended by ITTC 1957 (Eq. (2)) and with data reported by Demirel *et al.,* [18] in which a KCS ship was simulated at Re 2.2 x 10^9 and 2.7 x 10^9 using STAR-CCM$^+$ software. Table 6 presents the percentage difference in the friction resistance coefficient (C_F) as a function of Reynolds number (C_F = f (Re) between the CFD simulation results and the ITTC 1957 calculations, as well as the CFD simulations conducted by Demirel *et al.,* [18] for full-scale KCS ships without roughness (SSS).

Table 6
Comparison of the C_F of KCS ship CFD results with ITTC and Demirel for surfaces without roughness

Speed (knots)	Re	C_F x 10^3			ΔC_F (CFD-ITTC) (%)	ΔC_F (CFD-Demirel) (%)
		CFD	ITTC	Demirel *et al.,*[18]		
5	5.7 x 10^8	1.726	1.643	-	5.053	-
15	1.7 x 10^9	1.494	1.433	-	4.232	-
19	2.2 x 10^9	1.458	1.394	1.452	4.625	0.440
24	2.7 x 10^9	1.419	1.356	1.421	4.642	0.133

Table 6 shows that the C_F value derived from CFD simulation results, the empirical formula recommended by ITTC 1957 for flat plate and Demirel *et al.,*[18] exhibits a consistent decrease with increasing ship speed. The average percentage difference between the CFD and ITTC 1957 results is 4.41%, while the average percentage difference between the CFD simulation results and Demirel *et al.,* [18] research is 0.38%. Because the percentage of ΔC_F is very small, hence the CFD results in this study are adequate and acceptable. The CFD results are larger than ITTC 1957 for flat plate, which can be expected because the CFD results include 3D effects (form factor).

3. Result and Discussion

3.1 Friction Resistance

Table 7 summarizes the friction resistance coefficient C_F for different roughness arrangements and two Reynolds numbers, Re = 2.2 x 10^9 and 2.7 x 10^9. Table 7 shows that the smooth surface has the lowest C_F, namely 1.458 x 10^{-3} for Re = 2.2 x 10^9 and 1.419 x 10^{-3} for Re = 2.7 x 10^9. Further, for the smooth surface, C_F decreases with increasing Re [36, 37]. Re represents the combined effect of inertial and viscous forces. As Re increases beyond the critical value for transition, turbulence is observed, which indicates that inertial and viscous forces still exist, but the viscous force decreases and results in a decrease in C_F.

For the homogeneous roughness, C_F increases with increasing k_s [15], as expected. Further, C_F increases with increasing Re. This observation is consistent with the results obtained by Song *et al.,* [37]. The explanation for this phenomenon is that an increase in k_s leads to an increase in boundary layer thickness (δ). This increase in δ leads to greater momentum loss, thus C_F increases.

The same phenomenon is observed in the case of inhomogeneous roughness, where C_F increases with increasing Re. The order of C_F from lowest to highest is PQR < PRQ < QPR < QRP < RPQ < RQP. These results are in agreement with the findings of Suastika *et al.,* [14]. The C_F of the PQR model is the lowest among the other inhomogeneous arrangements, and the RQP has the highest C_F. This is due to the complex effect on the boundary layer interaction and the sudden change in k_s that causes a sharp change in the mean velocity profile [38]. To illustrate, in the PQR model, the flow velocity progresses from the fore-hull, which exhibits the lowest k_s (P), to the midship area, which has a higher k_s (Q), and finally to the aft-hull region with the highest k_s (R). When the flow transitions from low k_s

to higher k_s, there is an increase in the velocity profile and a decrease in turbulence, indicating a decrease in C_F. Conversely, when the flow transitions from a high to a low k_s (RQP), there is a decrease in velocity profile as turbulence increases in each transition section from R to Q, and Q to P. This results in an increase in the C_F.

Table 7
The C_F in KCS smooth, homogeneous roughness, and inhomogeneous roughness conditions

Roughness condition	$C_F \times 10^3$	
Smooth	Re = 2.2 x 10^9	Re = 2.7 x 10^9
SSS	1.458	1.419
Homogeneous	Re = 2.2 x 10^9	Re = 2.7 x 10^9
PPP	1.483	1.961
QQQ	2.135	2.183
RRR	2.291	2.318
Inhomogeneous	$C_F \times 10^3$	
	Re = 2.2 x 10^9	Re = 2.7 x 10^9
PQR	2.088	2.119
PRQ	2.089	2.136
QPR	2.090	2.146
QRP	2.092	2.146
RPQ	2.093	2.153
RQP	2.097	2.155

A comparison of the friction resistance coefficients for KCS smooth condition (S), with homogeneous roughness (H), and with inhomogeneous roughness (IH) can be seen in Tables 8 and 9 respectively. Table 8 demonstrates that as the roughness level increases, the difference in C_F between the homogeneous roughness condition and the smooth condition also increases. The maximum value for this difference is 36.34 % for the RRR condition (Re = 2.2 x 10^9) for homogeneous roughness, and 38.78 % for the RRR condition (Re = 2.7 x 10^9).

Table 9 presents the C_F difference between KCS in the smooth condition and inhomogeneous roughness. The average percentage value for this difference is 33.76%. The RQP arrangement shows the highest value of 34.14% which is higher than KCS in the smooth condition (Re = 2.7 x 10^9). The shear stress on a surface with homogeneous roughness is illustrated in Figure 5.

Table 8
Comparison of the ΔC_F (%) at smooth conditions and homogeneous roughness for Re = 2.2 x 10^9 and 2.7 x 10^9

Roughness arrangement	$\Delta C_{F\ (H-S)}$ (%) Re = 2.2 x 10^9	$\Delta C_{F\ (H-S)}$ (%) Re = 2.7 x 10^9
	SSS	SSS
PPP	1.62	27.63
QQQ	31.69	34.98
RRR	36.34	38.78

Table 9
Comparison of the ΔC_F (%) at smooth conditions and inhomogeneous roughness for Re = 2.2 x 10^9 and 2.7 x 10^9

Roughness arrangement	$\Delta C_{F\ (IH-S)}$ (%) Re = 2.2 x 10^9	$\Delta C_{F\ (IH-S)}$ (%) Re = 2.7 x 10^9
	SSS	SSS
PQR	30.16	33.04
PRQ	30.17	33.57
QPR	30.20	33.86
QRP	30.30	33.87
RPQ	30.32	34.08
RQP	30.16	34.14

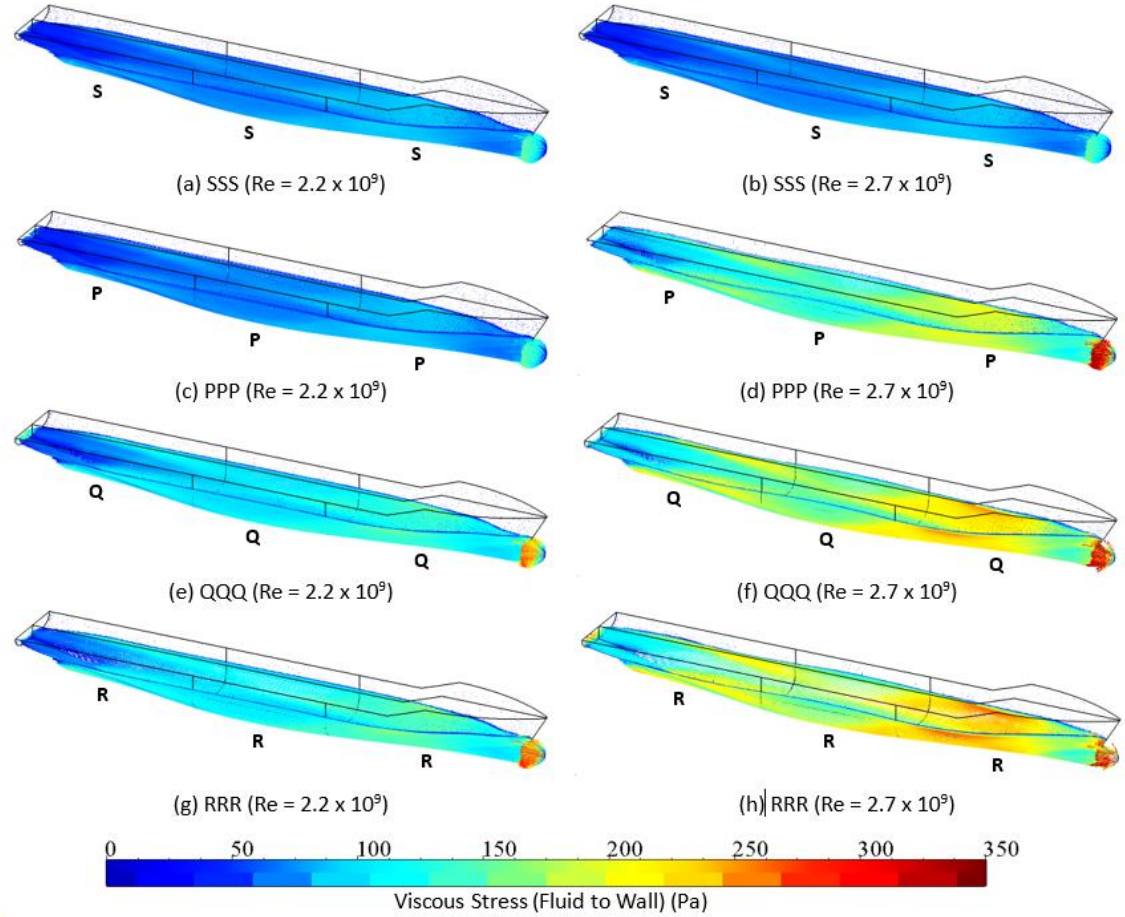

Fig. 5. Shear stress distribution on the hull surface for homogeneous roughness arrangements

Figure 5 shows that the shear stress increases as k_s and Re increase, supporting the C_F in Table 7 for homogeneous roughness conditions. However, this is not the case for the smooth condition, where, as the shear stress increases with increasing Re, the C_F value decreases because the velocity profile reaches the free stream velocity faster. Consequently, there is a slight loss of momentum, resulting in a smaller C_F at higher Re [15]. At lower Reynolds numbers for SSS and PPP, unique phenomena can be observed. The shear stress distribution is nearly identical for both, which can be attributed to the low turbulence and the dominant influence of viscosity influenced by the form factor of the hull. This phenomenon is in line with the results of the study by Yanuar *et al.,* [39]. Consequently, there is a minimal difference in C_F between SSS and PPP at lower Re, amounting to

1.71% for Re = 2.7 x 10^9. The impact of alterations in surface roughness on shear stress can be observed in Figure 6.

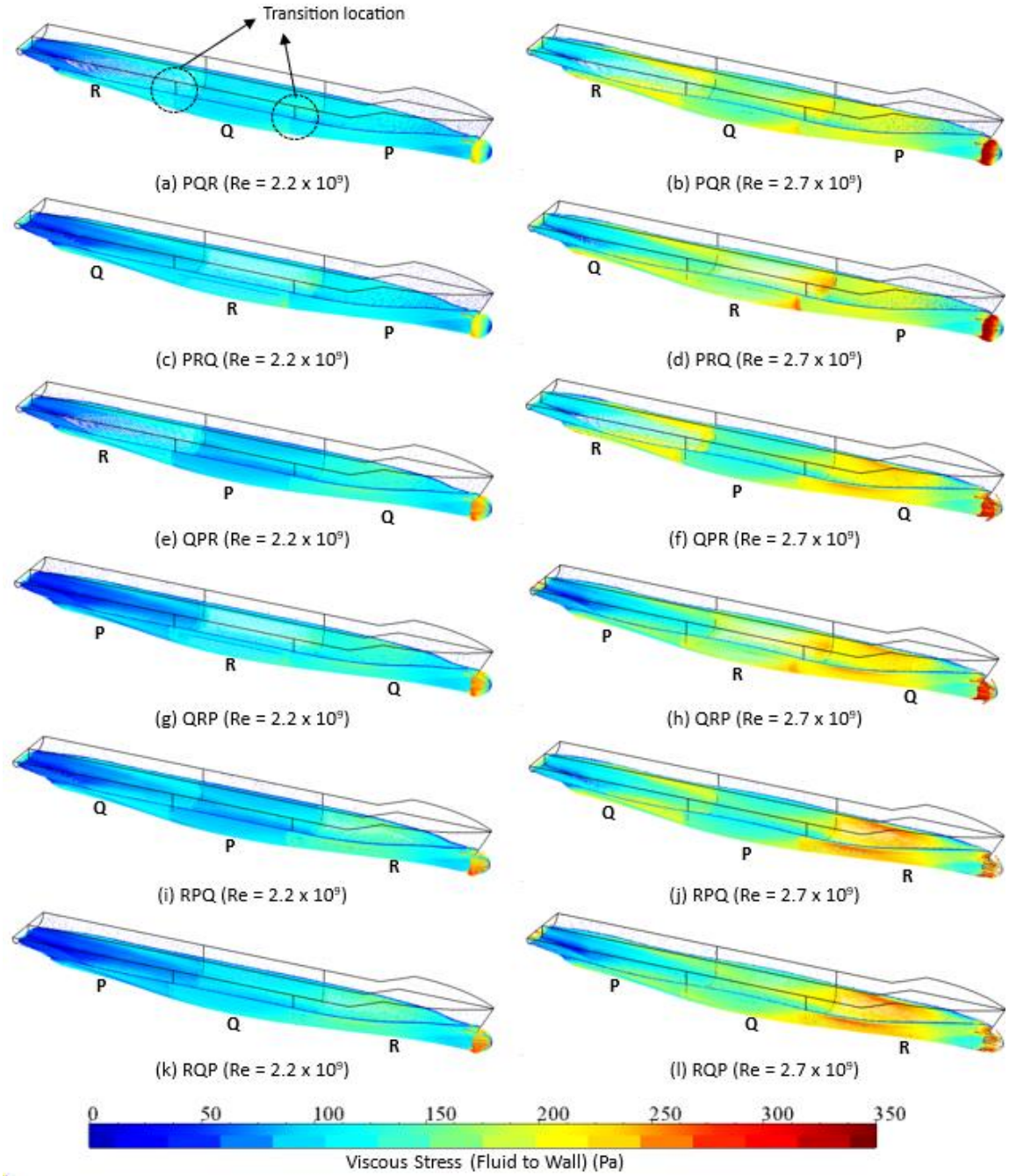

Fig. 6. Shear stress distribution on the hull surface for inhomogeneous roughness arrangements

Figure 6 shows the change in shear stress at the k_s transition of the inhomogeneous roughness. Figure 6 shows that the shear stress increases as Re is increased from 2.2 x 10^9 to Re 2.7 x 10^9 (which is indicated by the more dominant yellow to red contours at higher Re). An interesting point is the transition location. Figure 6 (a) and Figure 6 (b) show a significant increase in shear stress at the transition locations section (fore-hull to midship transition, and midship to aft-hull transition). This is due to the transition from lower k_s to higher k_s, so that the velocity increases [40] which indicates a decrease in C_F. This also causes PQR to have the smallest C_F among other inhomogeneous roughness models. On the contrary, in Figure 6 (k) and (l) there is a decrease in shear stress in each transition

location, so the turbulence continues to increase until the aft-hull segment which causes the RQP model to have the highest C_F. Fluctuations in shear stress distribution at each transition occur in Figure 6 (c), (d), (e), (f), (g), (h), (i), and (j), where respectively in the fore-hull to midship transition, and midship to aft-hull transition, there is a sharp change if there is a transition from low k_s to higher k_s, otherwise the shear stress will decrease when transitioning from high k_s to lower k_s.

3.2 Wave Resistance

Wave resistance is the transfer of energy by a ship to create waves at the free surface. A comparison of the wave resistance coefficient C_W for Froude number Fr = 0.2 and 0.25 (Re = 2.2 x 10^9 and 2.7 x 10^9) for smooth, homogeneous, and inhomogeneous roughness, is shown in Table 10.

Table 10
Wave resistance coefficient C_W for smooth, homogeneous, and inhomogeneous roughness conditions

Roughness condition	C_W x 10^3	
Smooth	Fr = 0.2 (Re = 2.2 x 10^9)	Fr = 0.2 5 (Re = 2.7 x 10^9)
SSS	0.212	0.667
Homogeneous	Fr = 0.2 (Re = 2.2 x 10^9)	Fr = 0.2 5 (Re = 2.7 x 10^9)
PPP	0.231	0.475
QQQ	0.164	0.561
RRR	0.191	0.665
Inhomogeneous	C_W x 10^3	
	Fr = 0.2 (Re = 2.2 x 10^9)	Fr = 0.2 5 (Re = 2.7 x 10^9)
PQR	0.211	0.664
PRQ	0.223	0.561
QPR	0.223	0.657
QRP	0.148	0.519
RPQ	0.187	0.578
RQP	0.176	0.550

Table 10 shows that for the smooth surface, C_W increases if Fr increases from 0.2 to 0.25. In sub-section 3.1 C_F decreases if Fr increases from 0.2 to 0.25. C_F due to the increase in velocity results in a reduction in viscous force due to an increase in the wave elevation [12, 18]. Consequently, C_W increases at higher Fr on a smooth surface. A similar phenomenon is observed in homogeneous roughness, where an increase in C_W is observed when Fr is increased. It can be observed that when Fr = 0.25, C_W increases with increasing k_s.

For the inhomogeneous roughness, the value of C_W increases with increasing Fr. At Fr 0.2, it can be observed that the RQP model with the maximum C_F among other models has the lowest C_W value, while the PRQ and QPR models have the maximum C_W value. This is due to a transition from the surface with the lowest k_s (P) to the highest k_s (R), resulting in a decrease in turbulence and a corresponding decrease in C_F. Consequently, the C_W composition of PQR and QPR is highest at Fr 0.2. In contrast, for Fr 0.25, the lowest C_W belongs to QRP, where the flow transitions from the surface with the greatest k_s (R) on the midship to the surface with the least k_s (P) on the aft-hull. This results in a pronounced decrease in the velocity in the aft-hull area and an enlargement of the wake field. The enlarged wake field is related to the surface pressure distribution on the aft-hull, which leads to an increase in the viscous pressure resistance C_{VP}. This causes the minimum C_W at QRP. The PQR at

Fr 0.25 exhibits the highest C_W among other inhomogeneous roughness models. This is due to the flow moving from the lowest k_s to the highest k_s towards the aft-hull, increasing the velocity when passing through the transition section indicated by the decrease in C_F. Consequently, the C_W increases to a maximum among other inhomogeneous roughness models. This explanation is in accordance with research by Bou-Zeid *et al.,* [38] and Song *et al.,* [37].

Figure 7 depicts the wave pattern around the KCS hull with inhomogeneous PQR roughness at Fr = 0.25. The coordinates (0.0) are set on the aft-hull and (1.0) on the fore-hull with Lpp = 230 m. It can be observed that on the fore-hull section, the wave system initiated by the initial disturbance begins with waves exhibiting an amplitude of 9.8 x 10^{-5} m, while on the fore-hull shoulder, a wave troughs with an amplitude of -9.8 x 10^{-5} m is formed. The negative sign on z/Lpp indicates that the wave is below the KCS waterline, while negative x/Lpp indicates the free surface area aft of the ship with a point (0.0) at the aft hull.

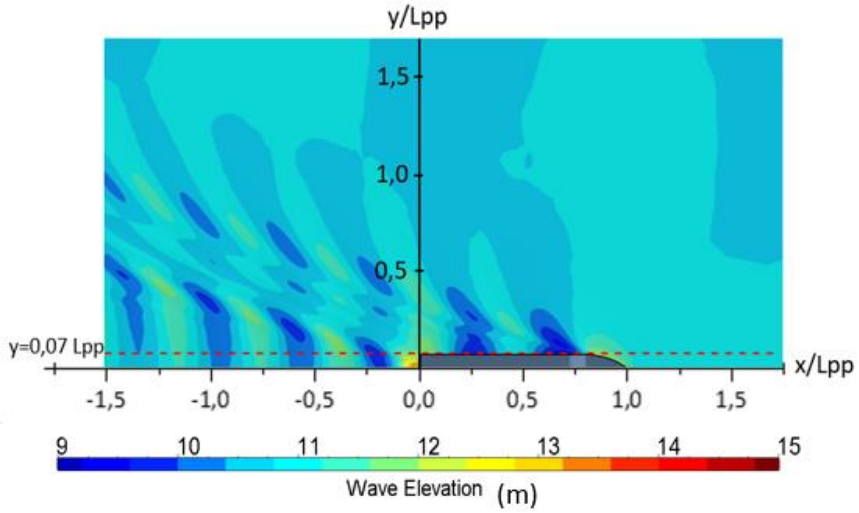

Fig. 7. Wave pattern around the KCS hull for PQR roughness arrangement

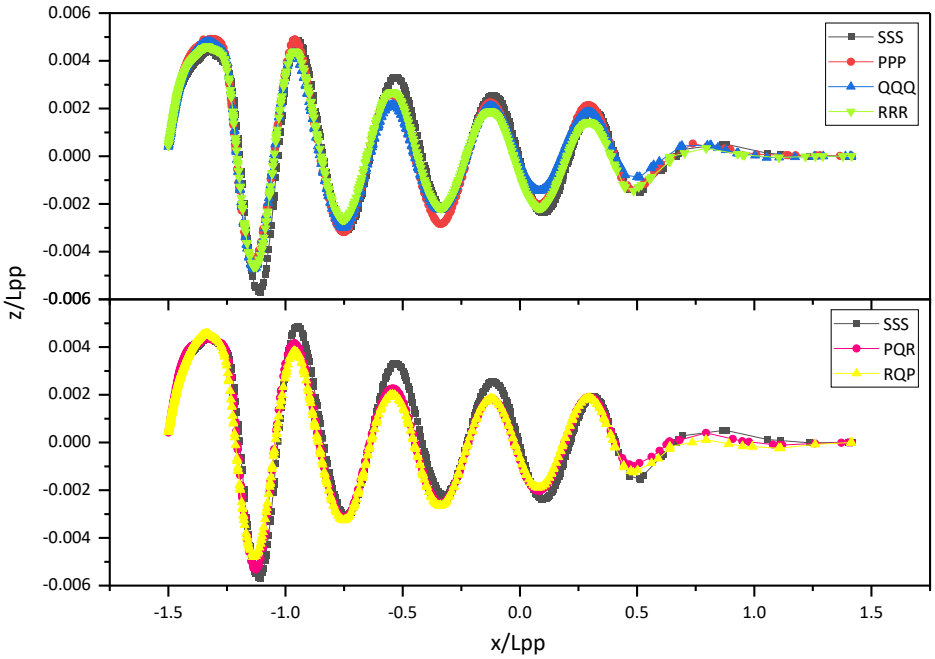

Fig. 8. Wave profiles of homogeneous (a), and inhomogeneous (b) roughness at y/Lpp = 0.07

To examine the specifics of the wave contours, Figure 8 depicts plots of the wave elevation along a line parallel to the ship (y/Lpp = 0.07) derived from the simulation. Figure 8 (a) depicts the KCS wave profile of a smooth surface and KCS with homogeneous roughness. It can be observed that the amplitude of the waves along the ship's hull appears to decrease as a consequence of the roughness effect. The significant reduction in the aft-hull wave system and the evident viscous effects on the wave resistance and wave system follow the findings of Raven *et al.,* [41]. Figure 8 (b) illustrates the wave profile for KCS smooth and with inhomogeneous roughness PQR (minimum C_F) and RQP (maximum C_F). It can be observed that the amplitude of the waves along the hull of PQR is greater than that of RQP. The smooth surface SSS exhibits the highest amplitude with the lowest C_F and the highest C_W.

3.3 Viscous Pressure Resistance

The boundary layer of the liquid affects both the virtual shape and the length of the body, as well as the pressure distribution in the aft-hull. As a result, a total force acts against the movement of the ship, a phenomenon called form resistance or viscous pressure resistance. Table 11 summarizes the viscous-pressure resistance coefficient C_{VP} for smooth, homogeneous, and inhomogeneous roughness.

Table 11
Viscous-pressure resistance coefficient CVP for smooth, homogeneous, and inhomogeneous roughness conditions

Roughness condition	C_{VP} x 10^3	
Smooth	Fr = 0.2 (Re = 2.2 x 10^9)	Fr = 0.25 (Re = 2.2 x 10^9)
SSS	0.146	0.142
Homogeneous	Fr = 0.2 (Re = 2.2 x 10^9)	Fr = 0.25 (Re = 2.2 x 10^9)
PPP	0.148	0.196
QQQ	0.214	0.218
RRR	0.229	0.232
Inhomogeneous	C_{VP} x 10^3	
	Fr = 0.2 (Re = 2.2 x 10^9)	Fr = 0.25 (Re = 2.2 x 10^9)
PQR	0.209	0.212
PRQ	0.209	0.214
QPR	0.209	0.215
QRP	0.209	0.215
RPQ	0.209	0.215
RQP	0.210	0.215

Table 11 shows that the C_{VP} value on the smooth surface decreases if Fr increases from 0.2 to 0.25. In homogeneous roughness, C_{VP} increases with increasing k_s and Fr. This phenomenon is also observed in inhomogeneous roughness, although C_{VP} remains relatively constant for all inhomogeneous conditions. The observed phenomenon can be attributed to a reduction in pressure recovery on the aft-hull, which in turn leads to an increase in C_{VP} as k_s and Fr increase.

3.4 Total Resistance

Table 12 summarizes the percentages of C_F, C_W, and C_{VP} in C_T for different surface conditions and Fr = 0.2 and 0.25 (Re = 2.2 x 10^9 and 2.7 x 10^9). To visualize the data, Figure 9 (a) and Figure 9 (b) show histograms of the resistance components for Fr = 0.2 (Re = 2.2 x 10^9) and Fr = 0.25 (Re = 2.7 x 10^9). Table 12 and Figure 9 (a) and Figure 9 (b) show that, for all surface conditions, the friction resistance (C_F) forms the dominant component of the ship total resistance (C_T), approximately 80% for the smooth surface, 82% for the homogeneous roughness, and 84% for the inhomogeneous roughness at Re = 2.2 x 10^9. As Re increases from 2.2 x 10^9 to 2.7 x 10^9, the percentage of the friction resistance decreases, while the percentage of the wave resistance increases. This finding is consistent with the results reported Oliveira *et al.,* [42]. Table 12 shows that for the smooth surface, the percentage of C_F decreases from approximately 80% to 64%, while the percentage of C_W increases from approximately 12% to 30%. For the homogeneous roughness, the percentage of C_F decreases from approximately 82% to 73%, while the percentage of C_W increases from approximately 9% to 19%. For the inhomogeneous roughness, the percentage of C_F decreases from approximately 84% to 73%, while the percentage of C_W increases from approximately 7.5% to 19.5%. These observations can be attributed to a change in the boundary layer and turbulence, and a change in the wave pattern when Re (or Fr) increases, which results in a decrease in C_F and an increase in C_W.

The viscous-pressure resistance decreases slightly as Re increases from 2.2 x 10^9 to 2.7 x 10^9. For the smooth surface, the percentage of C_{VP} decreases from approximately 8% to 6.4%, for the homogeneous roughness it decreases from approximately 8.3% to 7.3%, while for the inhomogeneous roughness it decreases from approximately 8.4% to 7.3%. A change in pressure distribution in the aft hull area of the ship contributes to a decrease in C_{VP}.

Figure 9 (a) and Figure 9 (b) show that, for the homogeneous roughness, C_F increases with increasing k_s, as expected (PPP < QQQ < RRR). For the inhomogeneous roughness, C_F increases slightly in the order PQR < PRQ < QPR < QRP < RPQ < RQP, which is consistent with the results reported by Suastika *et al.,* [14].

Table 12
The percentage of CF, CW, and CVP in CT for smooth, homogeneous, and inhomogeneous roughness conditions

Roughness condition	% C_F		% C_W		% C_{VP}	
Smooth	Re=2.2 x 10^9	Re=2.7 x 10^9	Fr = 0.2	Fr = 0.25	Fr = 0.2	Fr = 0.25
SSS	80.29	63.69	11.68	29.95	8.03	6.37
Homogeneous	Re=2.2 x 10^9	Re=2.7 x 10^9	Fr = 0.2	Fr = 0.25	Fr = 0.2	Fr = 0.25
PPP	79.64	74.51	12.40	18.04	7.96	7.45
QQQ	84.98	73.68	6.53	18.95	8.50	7.37
RRR	84.51	72.10	7.04	20.69	8.45	7.21
Inhomogeneous	Re=2.2 x 10^9	Re=2.7 x 10^9	Fr = 0.2	Fr = 0.25	Fr = 0.2	Fr = 0.25
PQR	83.26	70.77	8.41	22.16	8.33	7.08
PRQ	82.87	73.38	8.84	19.28	8.29	7.34
QPR	82.88	71.12	8.83	21.77	8.29	7.11
QRP	85.43	74.52	6.03	18.03	8.54	7.45
RPQ	84.09	73.09	7.50	19.60	8.41	7.31
RQP	84.48	73.80	7.08	18.82	8.45	7.38

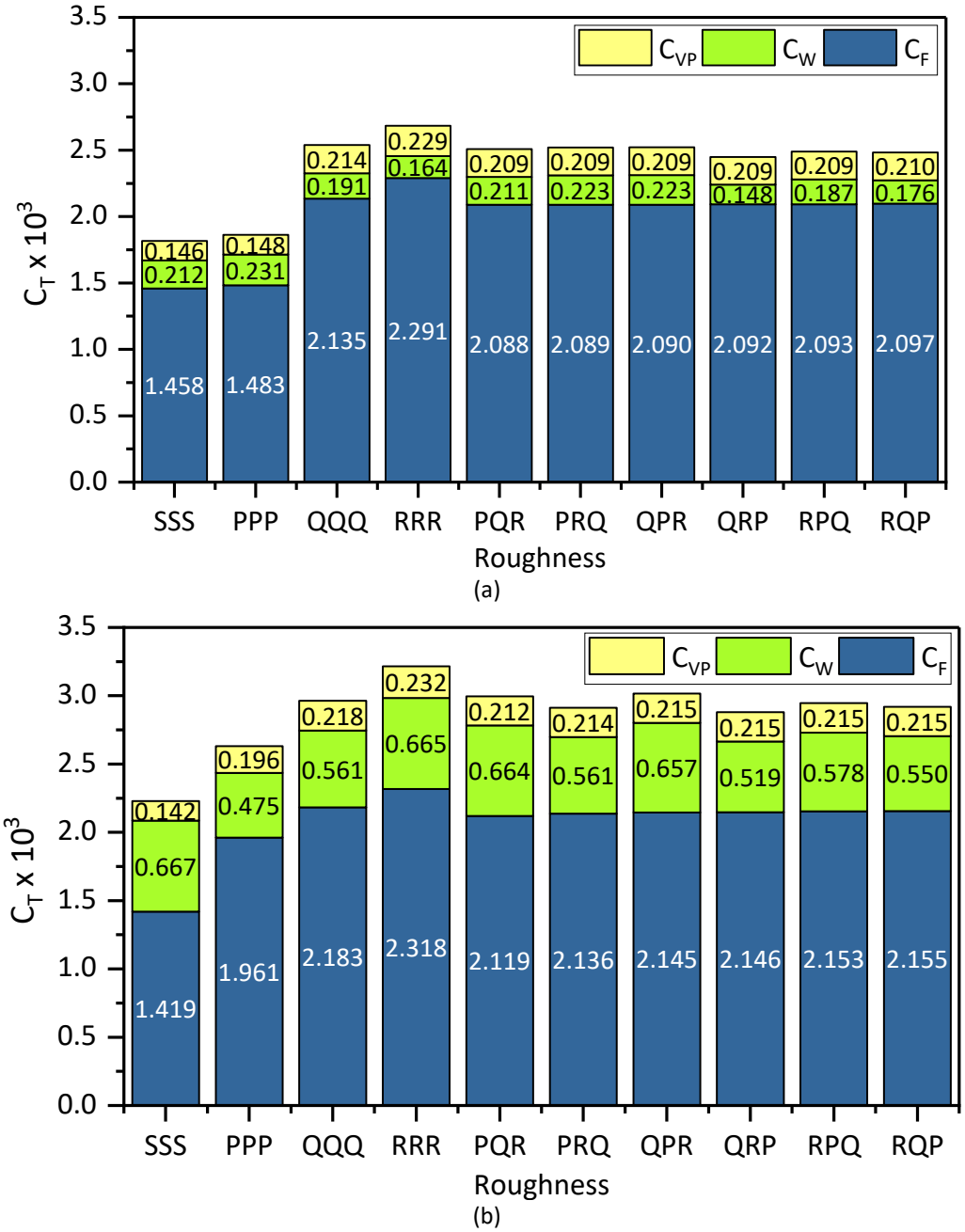

Fig. 9. (a) Components of C_T for different surface conditions at Fr = 0.2 (Re = 2.2 x 10^9), and (b) Components of C_T for different surface conditions at Fr = 0.25 (Re = 2.7 x 10^9)

4. Conclusion

The resistance force on the ship is the result of the pressure and shear stress distribution on the hull surface. An increase in surface roughness leads to an increase in the boundary-layer thickness, while the roughness distribution on the hull surface affects the ship total resistance. In this study a CFD method is utilized to investigate the effects of homogeneous and inhomogeneous surface roughness on the ship resistance, thereby investigating the various resistance components at two Froude numbers (Reynolds numbers), namely Fr = 0.2 and 0.25 (Re = 2.2 x 10^9 and 2.7 x 10^9). To model the inhomogeneous surface-roughness distribution, the ship hull is divided into three segments with equal surface area for all segments. A combination of three roughness heights is

investigated, denoted as P, Q, and R, which results in homogeneous and inhomogeneous roughness arrangements.

The findings show that surface roughness increases the ship total resistance, as expected (the smooth surface condition SSS has the lowest C_T among all surface conditions). For the homogeneous roughness condition, C_T increases with increasing k_s (PPP < QQQ < RRR). In all the cases considered, the friction resistance (C_F) is the dominant component of the total resistance, approximately 80% for the smooth surface, 82% for the homogeneous roughness, and 84% for the inhomogeneous roughness at Re = 2.2 x 10^9. As Re increases from 2.2 x 10^9 to 2.7 x 10^9, the percentage of the friction resistance decreases, while the percentage of the wave resistance increases. For the smooth surface, the percentage of C_W increases from approximately 12% to 30%, for the homogeneous roughness it increases from approximately 9% to 19%, and for the inhomogeneous roughness, it increases from approximately 7.5% to 19.5%. These findings are consistent with the results reported Oliveira *et al.,* [42]. Further, for the inhomogeneous roughness condition, C_F increases slightly in the order PQR < PRQ < QPR < QRP < RPQ < RQP for both Re = 2.2 x 10^9 and 2.7 x 10^9. This observation is consistent with the results reported by Suastika *et al.,* [14]. The viscous-pressure resistance decreases slightly as Re increases from 2.2 x 10^9 to 2.7 x 10^9. For the smooth surface, the percentage of C_{VP} decreases from approximately 8% to 6.4%, for the homogeneous roughness it decreases from approximately 8.3% to 7.3%, while for the inhomogeneous roughness it decreases from approximately 8.4% to 7.3%.

An increase in Re from 2.2 x 10^9 to 2.7 x 10^9 results in a decrease of percentage of C_F, increase of percentage of C_W, and a slight decrease of percentage of C_{VP} in their contribution to the total resistance C_T. These observations are attributed to the associated changes in the boundary layer and turbulence, alterations in the wave pattern, and alterations in pressure distribution in the aft hull area of the ship. These findings underscore the dynamic relationship between vessel speed (Fr and Re) and the various components of ship resistance. The CFD method utilized in this study provides valuable insight into the complex interactions between ship hull geometry, roughness distribution, and the resulting pressure and shear stress distribution on the hull surface.

Acknowledgement
The authors thank the DIKTI for the BPPDN scholarship, under contract numbers: T/56182/IT2/HK.00.01/2019 and 0626/E4/DT.04.02/2023.

Reference

[1] Brennan, Liam, and Philip Owende. "Biofuels from microalgae—a review of technologies for production, processing, and extractions of biofuels and co-products." *Renewable and sustainable energy reviews* 14, no. 2 (2010): 557-577. https://doi.org/10.1016/j.rser.2009.10.009

[2] Ketheesan, B., and N. Nirmalakhandan. "Development of a new airlift-driven raceway reactor for algal cultivation." *Applied Energy* 88, no. 10 (2011): 3370-3376. https://doi.org/10.1016/j.apenergy.2010.12.034

[3] Craggs, Rupert, Donna Sutherland, and Helena Campbell. "Hectare-scale demonstration of high rate algal ponds for enhanced wastewater treatment and biofuel production." *Journal of Applied Phycology* 24 (2012): 329-337. https://doi.org/10.1007/s10811-012-9810-8

[4] Oswald, W. J., M. Borowitzka, and L. J. Borowitzka. "Micro-algal biotechnology." *M. borowitzka and L borowitzka (Eds) Florida: CR Cpress* 315 (1988).

[5] Brune, D. E., G. Schwartz, A. G. Eversole, J. A. Collier, and T. E. Schwedler. "Intensification of pond aquaculture and high rate photosynthetic systems." *Aquacultural engineering* 28, no. 1-2 (2003): 65-86. https://doi.org/10.1016/S0144-8609(03)00025-6

[6] Chisti, Yusuf. "Biodiesel from microalgae." *Biotechnology advances* 25, no. 3 (2007): 294-306. https://doi.org/10.1016/j.biotechadv.2007.02.001

[7] Bosca, C., A. Dauta, and O. Marvalin. "Intensive outdoor algal cultures: How mixing enhances the photosynthetic production rate." Bioresource technology 38, no. 2-3 (1991): 185-188. https://doi.org/10.1016/0960-8524(91)90152-A

[8] Goldman, Joel C. "Outdoor algal mass cultures—II. Photosynthetic yield limitations." *Water Research* 13, no. 2 (1979): 119-136. https://doi.org/10.1016/0043-1354(79)90083-6
[9] Terry, Kenneth L., and Lawrence P. Raymond. "System design for the autotrophic production of microalgae." *Enzyme and microbial technology* 7, no. 10 (1985): 474-487. https://doi.org/10.1016/0141-0229(85)90148-6
[10] Yang, Zifeng, Matteo Del Ninno, Zhiyou Wen, and Hui Hu. "An experimental investigation on the multiphase flows and turbulent mixing in a flat-panel photobioreactor for algae cultivation." *Journal of applied phycology* 26 (2014): 2097-2107. https://doi.org/10.1007/s10811-014-0239-0
[11] Wu, L. B., and Y. Z. Song. "Numerical investigation of flow characteristics and irradiance history in a novel photobioreactor." *African Journal of Biotechnology* 8, no. 18 (2009.
[12] Liffman, Kurt, David A. Paterson, Petar Liovic, and Pratish Bandopadhayay. "Comparing the energy efficiency of different high rate algal raceway pond designs using computational fluid dynamics." *Chemical Engineering Research and Design* 91, no. 2 (2013): 221-226. https://doi.org/10.1016/j.cherd.2012.08.007
[13] Xu, Ben, Peiwen Li, and Peter Waller. "Study of the flow mixing in a novel ARID raceway for algae production." *Renewable energy* 62 (2014): 249-257. https://doi.org/10.1016/j.renene.2013.06.049
[14] Hreiz, Rainier, Bruno Sialve, Jérôme Morchain, Renaud Escudié, Jean-Philippe Steyer, and Pascal Guiraud. "Experimental and numerical investigation of hydrodynamics in raceway reactors used for algaculture." *Chemical Engineering Journal* 250 (2014): 230-239. https://doi.org/10.1016/j.cej.2014.03.027
[15] Dodd, Joseph C. "Elements of pond design and construction." In *Handbook of Microalgal Mass Culture (1986)*, pp. 265-284. CRC Press, 2017.
[16] Moulick, Sanjib, BvC Mal, and S. Bandyopadhyay. "Prediction of aeration performance of paddle wheel aerators." *Aquacultural Engineering* 25, no. 4 (2002): 217-237. https://doi.org/10.1016/S0144-8609(01)00087-5
[17] Ahmad, Taufik, and Claude E. Boyd. "Design and peroormance of paddle wheel aerators." *Aquacultural Engineering* 7, no. 1 (1988): 39-62. https://doi.org/10.1016/0144-8609(88)90037-4.
[18] Kommareddy, Anil R., and Gary A. Anderson. "Mechanistic modeling of a Photobioreactor system." In *2005 ASAE Annual Meeting*, p. 1. American Society of Agricultural and Biological Engineers, 2005.
[19] Camacho, F. García, A. Contreras Gomez, T. Mazzuca Sobczuk, and E. Molina Grima. "Effects of mechanical and hydrodynamic stress in agitated, sparged cultures of Porphyridium cruentum." *Process Biochemistry* 35, no. 9 (2000): 1045-1050. https://doi.org/10.1016/S0032-9592(00)00138-2
[20] Hondzo, Midhat, and Dennis Lyn. "Quantified small-scale turbulence inhibits the growth of a green alga." *Freshwater Biology* 41, no. 1 (1999): 51-61. https://doi.org/10.1046/j.1365-2427.1999.00389.x
[21] Al-Homoud, Amer, and Miki Hondzo. "Energy dissipation estimates in oscillating grid setup: LDV and PIV measurements." *Environmental Fluid Mechanics* 7 (2007): 143-158. https://doi.org/10.1007/s10652-007-9020-0